CFD Analysis of Magnetic Bearing Instability of S-CO_2 Turbomachinery

Yong Jae Chae, Do Kyu Kim, Jeong Ik Lee
Nuclear & Quantum Engr. Dept. KAIST
**Corresponding author: jeongiklee@kaist.ac.kr*

1. Introduction

Recently the Micro Modular Reactor(MMR) has become an issue that can replace the ship's diesel engine, and is under research and development by KAIST research team. MMR is a 12MWe fast factor that uses supercritical CO_2(S-CO_2) as a coolant and working fluid. The advantages are that it can be installed anywhere and it can be used for distributed power generation. Thus, power can be supplied to the isolated place [1].

In the case of MMR, a magnetic bearing is suitable for S-CO_2 turbomachinery. For 10MWe system, the gas foil bearing has insufficient load capability and oil lubricated bearing involves CO_2 purity control problem (Fig. 1). Thus, magnetic bearing is chosen for the MMR to support the shaft without load and purity problems.

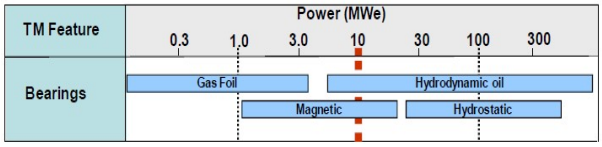

Fig 1. Bearing Options for S-CO_2 Brayton Cycles with various power scales [2]

The magnetic bearing test was conducted at KAERI. There were able to observe instability of the shaft position control in the S-CO_2condition while the bearing showed stable operation under atmospheric condition. The causes are expected to be high-pressure high-density fluid around the shaft. Furthermore, rapid density change of S-CO_2 is expected to induce instability. Therefore, there were a prior study on the instability of magnetic bearing operating under S-CO_2 conditions [3]. The analytic solution from a simplified Reynolds equation was applied assuming axial direction force is negligible and the acts at steady rotation. The Reynolds equation is as follows.

$$\frac{\partial}{\partial x}\left(\frac{\rho h^3}{12\mu}\frac{\partial p}{\partial x}\right) = \frac{1}{2}\frac{\partial(\rho h\mu)}{\partial x}$$

(X: circumferential direction, u: circumferential velocity, h: gap, ρ: density, μ: viscosity)

The Ng-Pan model was used for the turbulent lubrication model. Therefore, the turbulence effect can be considered by a coefficient k_x, which is expressed as $k_x = 12 + K_x(Re)^{n_x}$ instead of 12 in the left side of the equation.

First, the initial supply pressure and temperature were assumed to be uniform. The material properties from initial condition are substituted for the Reynolds equation to obtain the pressure. The iterative calculation was performed until the pressure was converged to obtain. Operating condition range of the model is shown in Table1. The eccentricity, ε is the ratio between the unbalanced length(e) and the averaged gap distance (c = $R_2 - R_1$). The geometry is described in Fig2.

Table 1. Operation condition range of the model

Supply temperature	10 ~ 50℃
Supply pressure	1 ~ 100bar
Rotational speed	10000 ~ 30000RPM
Eccentricity, ε	0.25 ~ 0.75

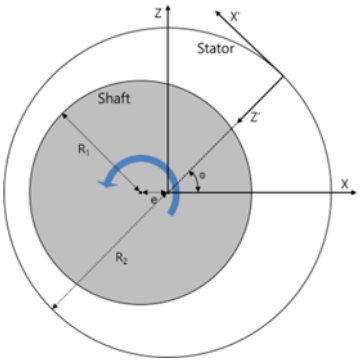

Fig 2. Geometry of the unbalanced shaft and the stator

From the F_x contour for various thermal conditions were obtained from the previous study [3], the operating conditions near the pseudo-critical point is expected to have high disturbance force due to the fluid. Furthermore, the force is sensitive to the temperature and small change in temperature can result in large force. Therefore, heat transfer analysis model is additionally needed. In this paper, heat transfer analysis model is added through CFD modeling in the STAR CCM+ program to study the effect on the bearing instability. The pressure distribution and force from CFD model is compared with that from the model developed in prior study. It is noted that the presented results are preliminary results and more refinement is needed in the near future to draw any conclusion.

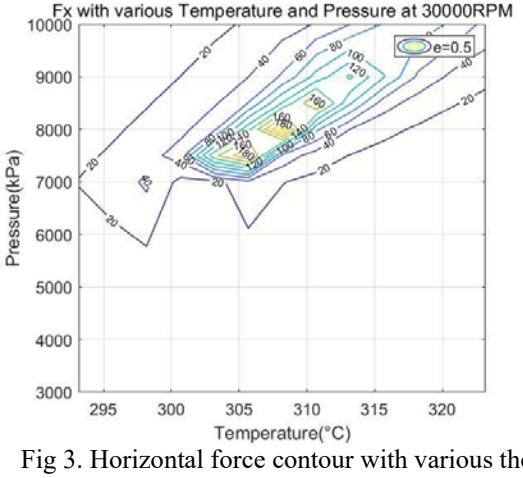

Fig 3. Horizontal force contour with various thermal condition, 30000RPM, ε=0.5

2. Method and results

2.1 CFD modeling - geometry

STAR CCM+ is used for the analysis. First, the geometry of shaft, bearing and fluid are modeled. To analyze the heat transfer of the wall and the fluid between bearing and shaft, the geometry is assumed to be a co-centric cylinder. The shaft is shown in shaded are in it is unbalanced from the center as shown in Fig 5.

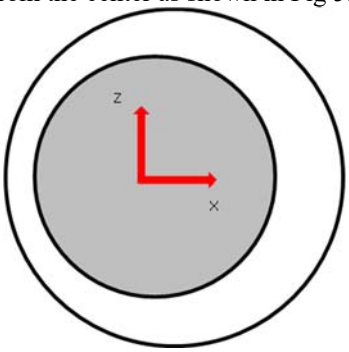

Fig 4. Cross-sectional view of CFD model

Fig 5. Geometry of CFD model

The radius of inner surface(shaft) is 0.032m, outer surface(bearing) is 0.0324m, clearance is 400 μm. This data of the geometry is referred from the prior study. .

2.2 CFD modeling – meshing and continua

Prism layer meshes are used near the boundary and polygonal meshes are used for the rest of the remaining fluid domain as shown in Figs. 6 & 7.

The edge length before mesh refinement was $1.2 * 10^{-5}$m. Surface growth rate that determines the rate at which face edge sizes vary from one face to its neighbor is 1.1. The minimum surface size which value specifies the lower limit of edge lengths on the surface mesh was $4.0 * 10^{-7}$m. The number of prism layer meshes was set to 10 and prism layer stretching was set to 1.5. The stretching factor is the ratio of the thickness of a cell layer to the thickness of the preceding layer. The total thickness of the prism layer was $2.0 * 10^{-6}$m. 65,000 cells in total was generated with these settings.

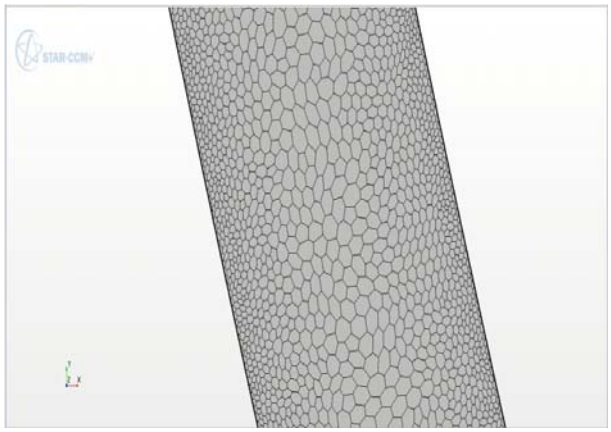

Fig 6. Polygonal meshes of CFD model

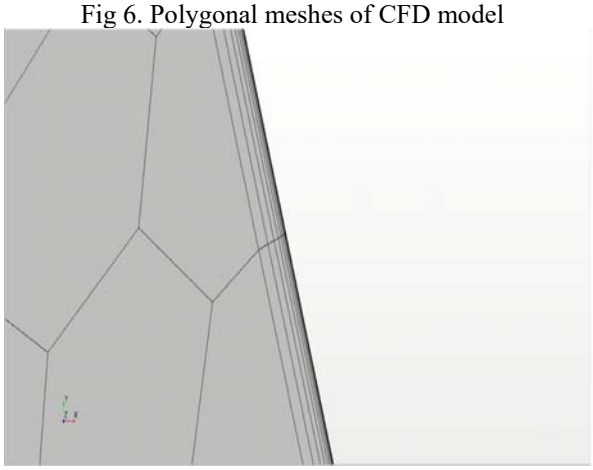

Fig 7. Prism layer meshes of CFD model

Reynolds averaged Navier-Stokes equation with SST(Menter) K-Omega turbulence model was used for the turbulence model. Pressure and temperature were set to 5MPa and 25℃ respectively for the first case and 8MPa and 40℃ for the second case. The properties of CO_2 in each case are obtained from NIST PREPROP.

Outer and inner surfaces were set to wall boundary condition and only inner surface rotates at 30,000RPM. The thermal specification of outer surface is constant temperature. The type of inlet and outlet boundary conditions were mass flow inlet and pressure outlet, respectively. The mass flow rate was set to 0.005kg/s for each case.

The convergence criteria were set to when residuals of mass, momentum, energy are below 10^{-6}.

2.3 CFD modeling – results

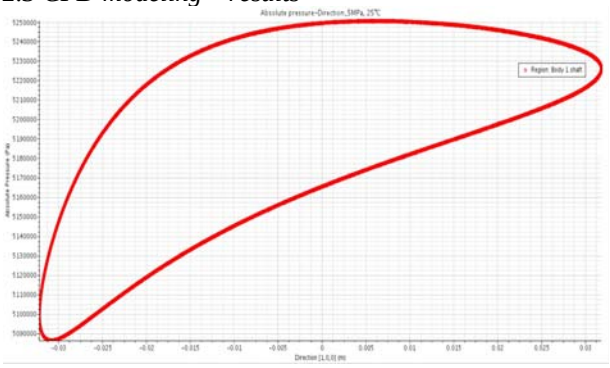

Fig 8. Absolute pressure-Direction plot_5MPa, 25℃

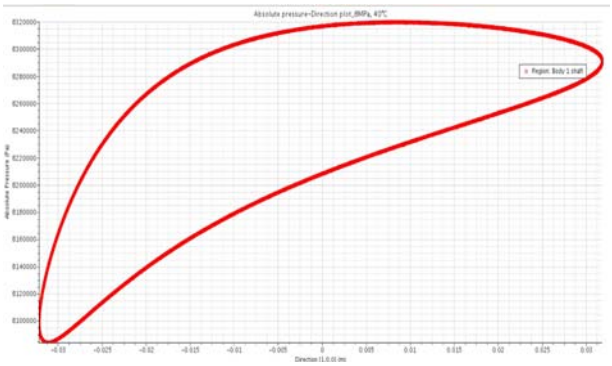

Fig 9. Absolute pressure-Direction plot_8MPa, 40℃

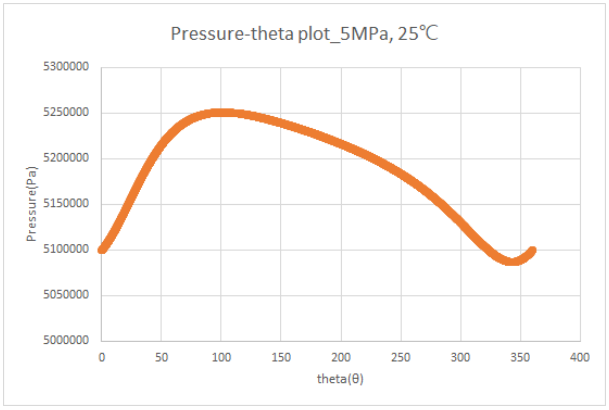

Fig 10. Pressure-theta plot_5MPa, 25℃

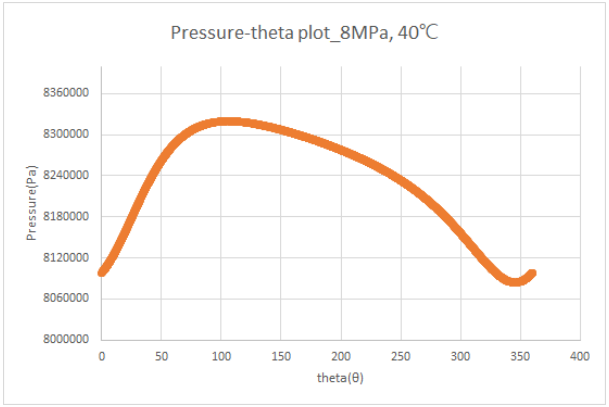

Fig 11. Pressure-theta plot_8MPa, 40℃

From pressure-theta plot in Figs. 10 & 11, the net horizontal and vertical forces of each case are obtained. In the first case, the net horizontal and vertical forces are 767.7N and -647.2N, respectively. The negative sign means downward direction. The net force direction is -40°. In the second case, the net horizontal and vertical forces are 1167.3N and -832.3N, respectively. This force direction is -35°.

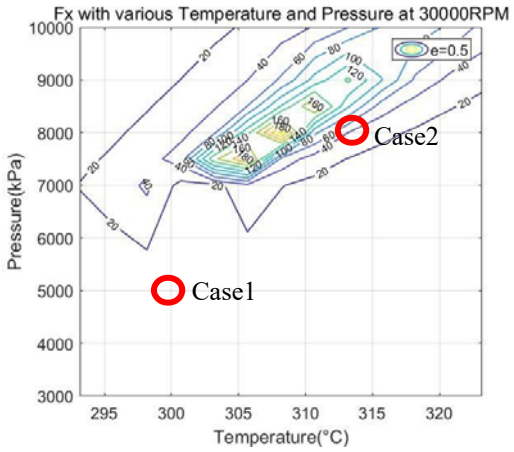

Fig 12. F_Z contour with various thermal condition, 30000RPM, ε=0.5

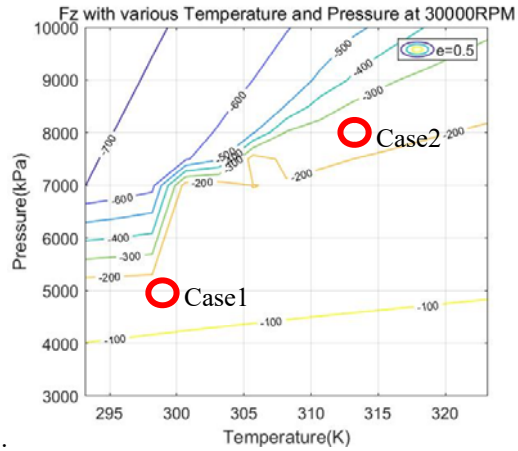

Fig 13. F_X contour with various thermal condition, 30000RPM, ε=0.5

In comparison with analytic solution of the prior study in Figs. 11 & 12, the force direction and pressure distribution are similar. However, the magnitudes are substantially different. Two reasons are expected to affect such discrepancy. First, this study applied different turbulence model from that of the prior study. The current model used SST K-Omega model that solved two partial differential equation in contrast to the prior study which used simplified Ng-Pan turbulence model. Next, 3D effect as well as the heat transfer modeling are expected to cause such difference.

In the near future, more accurate CO2 properties will be implemented as well as sensitivity to the boundary conditions will be studied.

3. Conclusions

In comparison with the analytic solution, the force direction obtained from the CFD modeling with more accurate turbulence model, 3D effect and heat transfer is similar. However, the magnitude is substantially different.

Further investigation will commence soon regarding the effect of boundary conditions and accuracy of CO2 properties.

Acknowledgement

Authors gratefully acknowledge that this research is funded by Saudi Aramco KAIST CO_2 Management Center.

REFERENCES

[1] Kim, S. G., Yu, H., Moon, J., Baik, S., Kim, Y., Jeong, Y. H., and Lee, J. I. (2017) A concept design of supercritical CO2 cooled SMR operating at isolated microgrid region. Int. J. Energy Res., 41: 512–525. doi: 10.1002/er.3633

[2] Sienicki, James J., et al. "Scale dependencies of supercritical carbon dioxide Brayton cycle technologies and the optimal size for a next-step supercritical CO2 cycle demonstration." *SCO2 power cycle symposium*. 2011

[3] Kim, D. K, Baik, S. J and Lee, J. I. "Instability study of magnetic journal bearing under supercritical CO_2 cooled MMR conditions" *Transactions of the Korean Nuclear Society Autumn Meeting.* 2018

[4] Dousti, Saeid, and Paul Allaire. "A compressible hydrodynamic analysis of journal bearings lubricated with supercritical carbon dioxide." *Proceeding of Supercritical CO2 Power Cycle Symposium, San Antonio, TX*. 2016.